IOPscience iopscience.iop.org

Home Search Collections Journals About Contact us My IOPscience

Injection-insensitive lateral divergence in broad-area diode lasers achieved by spatial current modulation

This content has been downloaded from IOPscience. Please scroll down to see the full text.

2016 Appl. Phys. Express 9 112102

(http://iopscience.iop.org/1882-0786/9/11/112102)

View the table of contents for this issue, or go to the journal homepage for more

Download details:

IP Address: 159.226.165.17
This content was downloaded on 02/07/2017 at 09:47

Please note that terms and conditions apply.

You may also be interested in:

Beam control of high-power broad-area photonic crystal lasers using ladderlike groove structure
Tao Wang, Lijie Wang, Shili Shu et al.

Control of lateral divergence in high-power, broad-area photonic crystal lasers
Jiamin Rong, Enbo Xing, Lijie Wang et al.

Experimental and theoretical study of finite-aperture tapered unstable resonator lasers
Martin Spreemann, Jörg Fricke, Hans Wenzel et al.

Experimental and theoretical analysis of the dominant lateral waveguiding mechanism in 975 nm high power broad area diode lasers
P Crump, S Böldicke, C M Schultz et al.

Angled cavity photonic crystal lasers with asymmetrical high-order surface gratings
Yun Liu, Yufei Wang, Hongwei Qu et al.

Radiative characteristics of semiconductor injection lasers based on narrow asymmetric waveguides
S D Chervinskii, B S Ryvkin, Yu M Shernyakov et al.

Efficiency-optimized monolithic frequency stabilization of high-power diode lasers
P Crump, C M Schultz, H Wenzel et al.

Comparative theoretical and experimental studies of two designs of high-power diode lasers
K H Hasler, H Wenzel, P Crump et al.

Applied Physics Express **9**, 112102 (2016)
http://doi.org/**10.7567/APEX.9.112102**

Injection-insensitive lateral divergence in broad-area diode lasers achieved by spatial current modulation

Tao Wang[1,2], Cunzhu Tong[1*], Lijie Wang[1], Yugang Zeng[1], Sicong Tian[1], Shili Shu[1], Jian Zhang[1], and Lijun Wang[1]

[1]*State Key Laboratory of Luminescence and Application, Changchun Institute of Optics, Fine Mechanics and Physics, Chinese Academy of Sciences, Changchun 130033, China*
[2]*University of Chinese Academy of Sciences, Beijing 100049, China*

*E-mail: tongcz@ciomp.ac.cn

Received September 10, 2016; accepted October 4, 2016; published online October 20, 2016

High-power broad-area (BA) diode lasers often suffer from low beam quality, broad linewidth, and a widened slow-axis far field with increasing current. In this paper, a two-dimensional current-modulated structure is proposed and it is demonstrated that it can reduce not only the far-field sensitivity to the injection current but also the linewidth of the lasing spectra. Injection-insensitive lateral divergence was realized, and the beam parameter product (BPP) was improved by 36.5%. At the same time, the linewidth was decreased by about 45% without significant degradations of emission power and conversion efficiency. © 2016 The Japan Society of Applied Physics

High-power diode laser systems based on a broad-area (BA) diode laser are well-established laser sources for a variety of applications. The main advantages of such systems are high wall-plug efficiency, high optical power, reliability, long lifetime, relatively low cost, and small volume. However, besides these numerous advantages, the major drawbacks of high-power diode laser systems with BA diode lasers are their poor beam quality and low brightness. The cavity length and stripe width of a BA edge-emitting laser are many times larger than the lasing wavelength, meaning that the device is filled by a large number of supported optical modes[1)] and suffers from the time and space instabilities of the optical field. Typical phenomena include self-focusing,[2)] filamentation,[3)] thermal lensing,[4)] and the deteriorated lateral divergence with increasing injection current, i.e., the so-called far-field blooming.[5,6)]

The deterioration of the lateral beam quality of BA lasers limits their suitability for many potential applications. To solve this problem, some approaches were proposed, such as the use of unstable resonators,[7)] α-DFB lasers,[8)] a tapered or master oscillator power amplifier (MOPA) structure,[9,10)] a titled cavity,[11)] and a microstructure.[12)] These approaches can improve the beam quality, but do not provide sufficient help for the far-field blooming, which is mainly caused by the lateral carrier accumulation (LCA) at the device edges.[6)] Lateral gain tailoring[13–17)] can create an arbitrary two-dimensional carrier profile and hence suppress the LCA to improve the sensitivity of the far field to the injection current.[16,17)] On the basis of that, the high beam quality and low far-field dependence on the injection current in BA lasers obtained using ion implantation techniques was demonstrated.[16,17)] However, this method reduced the conversion efficiency owing to carrier loss at the implant-generated point defects near the active region, and enhanced self-heating and thermal lensing.[17)] In addition, implantation also increases the complexity and fabrication cost. Techniques that can suppress LCA without degrading efficiency are expected.

In this paper, we propose a new structure called the spatial-current-modulated (SCM) structure to adjust the carrier distribution and suppress the LCA. The periodical current profile along the lateral and longitudinal directions formed a two-dimensional current flow; thus, periodical gain loss was obtained, which will suppress the current spreading and reduce the carrier density at the mesa edges. The measured near and far fields demonstrated the feasibility of this structure. The lasing spectra were also measured and analyzed.

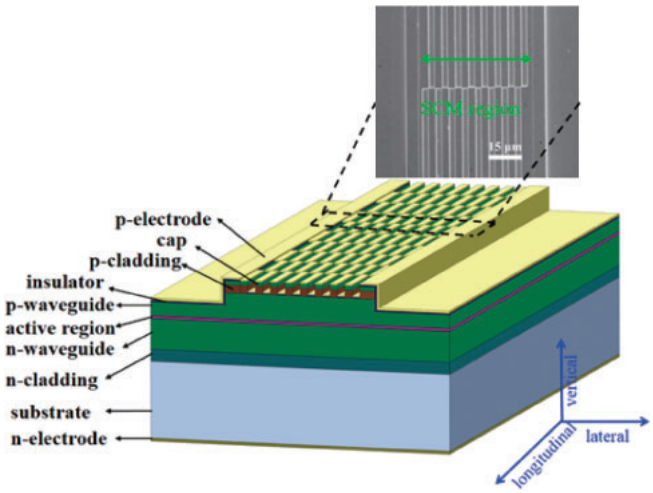

Fig. 1. Schematic diagram of the BA laser with SCM structure.

To better understand the mechanism and effectiveness of the proposed approach, the device structure is firstly described. In this work, the laser devices used two InGaAs quantum wells (QWs) emitting at 965 nm as the gain material. The active region was embedded in an asymmetric superlarge optical cavity (SLOC) consisting of 3.0 and 1.2 μm n- and p-type doped $Al_{0.1}Ga_{0.9}As$ waveguides. The cladding layers were 600 nm $Al_{0.15}Ga_{0.85}As$ and 550 nm $Al_{0.2}Ga_{0.8}As$ in the n- and p-type doped sides, respectively. The thickness of the heavily doped GaAs p-cap layer was 200 nm. After epitaxial growth by metal organic chemical vapor deposition (MOCVD), 64-μm-wide mesas were firstly fabricated by inductively coupled plasma (ICP) etching. Then, the SCM structure was defined on the stripe with a distance of 7 μm from each mesa edge, as indicated in Fig. 1. This SCM structure consists of a periodically distributed two-dimensional contact electrode array with a single electrode configuration of 3 μm width and 62 μm length. The distribution separations were $\Lambda_1 = 6\,\mu m$ and $\Lambda_2 = 124\,\mu m$ in the lateral and longitudinal directions, respectively. The etching depth for the electrode was 700 nm down to the poorly doped top cladding layer. Then, an electrical insulating layer was

© 2016 The Japan Society of Applied Physics

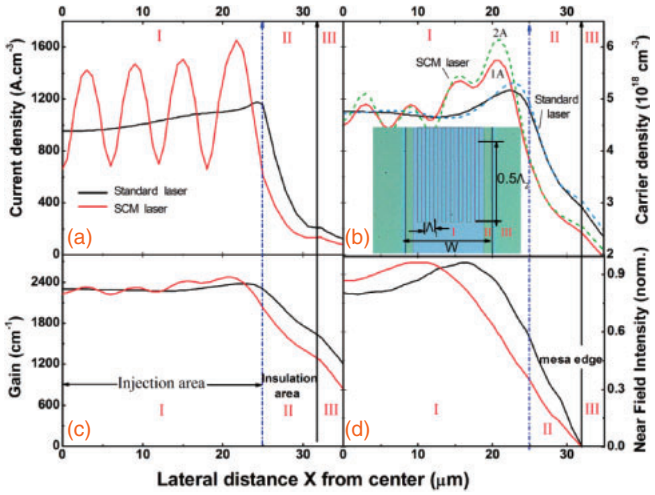

Fig. 2. Lateral distributions of (a) current density, (b) carrier density, (c) local gain, and (d) near-field intensity at 1 A injection current. The inset in (b) is a microphotograph of the SCM laser.

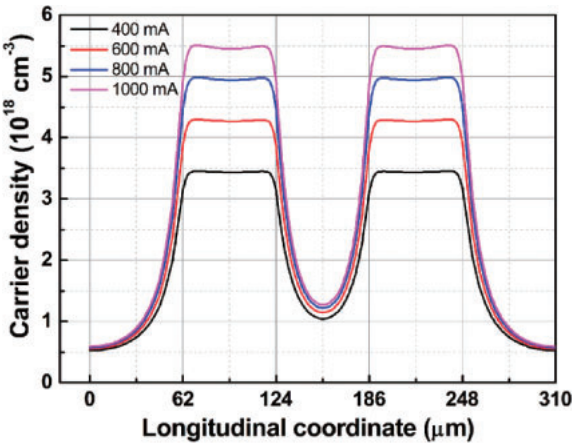

Fig. 3. Longitudinal carrier density profiles inside the top QW at injection currents of 0.4 A (black), 0.6 A (red), 0.8 A (blue), and 1.0 A (pink).

deposited and contact window opening was carried out, followed by p-side Ti–Pt–Au contact metal deposition, substrate thinning, and n-side AuGeNi–Au metal deposition. Finally, the wafer was cleaved into an individual diode laser with a cavity length of $L = 1.24$ mm. The laser devices were mounted epi-side down on a copper heat sink using indium solder without facet passivation or coating. Standard devices without microstructures with the same cavity length were also fabricated on the same sample for comparison.

To comprehensively understand the physical mechanisms of the SCM diode lasers, the current density, carrier distribution, gain profile, and intensity along the lateral direction were analyzed. The simulation software LASTIP for semiconductor lasers was utilized.[18] To simplify the analysis, only a half structure was simulated in the lateral direction (slow axis) considering the symmetry of SCM. All configuration parameters used remain consistent with the experimental devices described earlier. The top structure of the device was divided into three regions to simplify it. Regions I and II are located on the stripe and separated as injection and insulation areas, respectively. The injection area has the microstructures and metal contact, and the insulation area is near the stripe edge and is deposited with SiO_2. Region III is the nonstripe area. Figure 2(a) shows the current density within the top QW as a function of lateral position with the injection current of 1 A. As can be seen, the current density of the SCM laser is periodically modulated by the injection stripes. In Fig. 2(b), the carrier density near the edge of the injection area is much lower than that without a microstructure, even at the injection current of 2 A. The carrier density in the injection area is still modulated, but the amplitude becomes small. The carrier density is reduced to about 1×10^{18} cm^{-3} at the edge of the injection area owing to the SCM structure, and the scope of the fluctuation in the center region is only about 0.4×10^{18} cm^{-3}. By extending the effect of current modulation on the material gain, the effect becomes much gentler [Fig. 2(c)] with a fluctuation of $\sim$120 cm^{-1} in the center region. The low modulation intensity in the lateral direction is the key to improving the far-field blooming but without the penalty of emission performance.[16] The strong modulation will reduce significantly the modes, increase the threshold, and reduce the output power.[16] The decreased carrier density at the mesa edges will improve the dependence of the far field on the injection current.[6] It shows narrowing in the near-field profile in Fig. 2(d); thus, a more stable lateral far-field distribution is expected[19] in the SCM BA lasers.

The carrier density in the QW along the longitudinal direction without a lateral neighbor electrode was calculated and is shown in Fig. 3. The separation of injection and without injection in the longitudinal direction is 62 μm; thus, it shows a strong modulation of carrier density. The difference in carrier density between the injection area and the noninjection area is as large as 4.2×10^{18} cm^{-3} at 1 A and strongly dependent on the injection current. This modulation scope is over four times higher than that in the lateral direction at the same current, and hence it will form an evident alternate distribution of gain and absorption in the longitudinal direction. The high contrast in carrier density might be caused by the large separation of distributed electrode contact, and the etched trenches enhance this effect. The strong fluctuation of gain along the cavity direction will introduce loss to high-order longitudinal modes and reduce evidently the mode number.

Figure 4 shows the light–current–voltage (L–I–V) and power conversion efficiency (PCE) curves of the fabricated SCM and standard lasers. It can be seen that there is almost no large difference in the output performance of these two lasers before 2 A. The SCM laser shows a slightly higher voltage than the standard one; the corresponding values are 0.7 and 1.3% higher at 2 and 3 A, respectively. Both devices show similar conversion efficiencies up to 2 A; the highest PCEs are $\eta_E = 59.9$ and 62.4% for the SCM and standard devices, respectively. The decrease in the emission power of the SCM device at above 2 A might be due to the mode hopping.

To prove the stability of the far field, the current-dependent lateral divergence under CW operation for standard and SCM devices was measured and is shown in Fig. 5. As injection current is increased, the far-field distributions of the standard laser become worse and the lateral divergence reaches 10.2° at 2.5 A, which increases by almost 62%. In contrast, the lateral divergence of the SCM laser is quite sable; it increases by only 3%. Even at 2 A, the blooming is still less than 7%. Thus, the injection-insensitive lateral divergence is realized.

© 2016 The Japan Society of Applied Physics

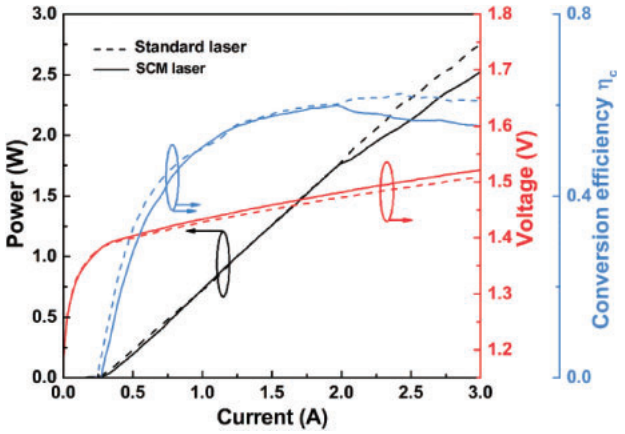

Fig. 4. *L–I–V* and wall-plug efficiencies of SCM lasers (solid line) and standard lasers (dashed line) under CW operation at a heat sink temperature of 20 °C.

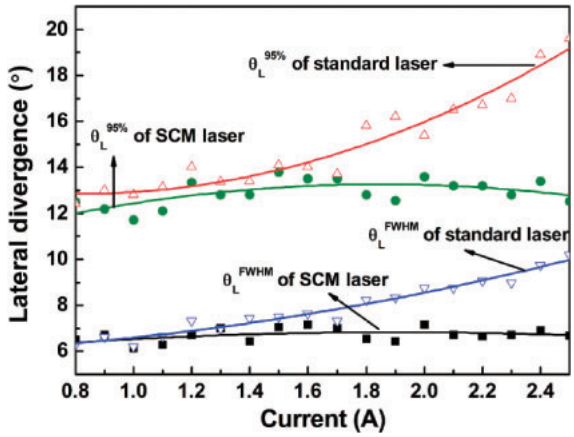

Fig. 5. Current-dependent lateral divergence for the standard and SCM lasers.

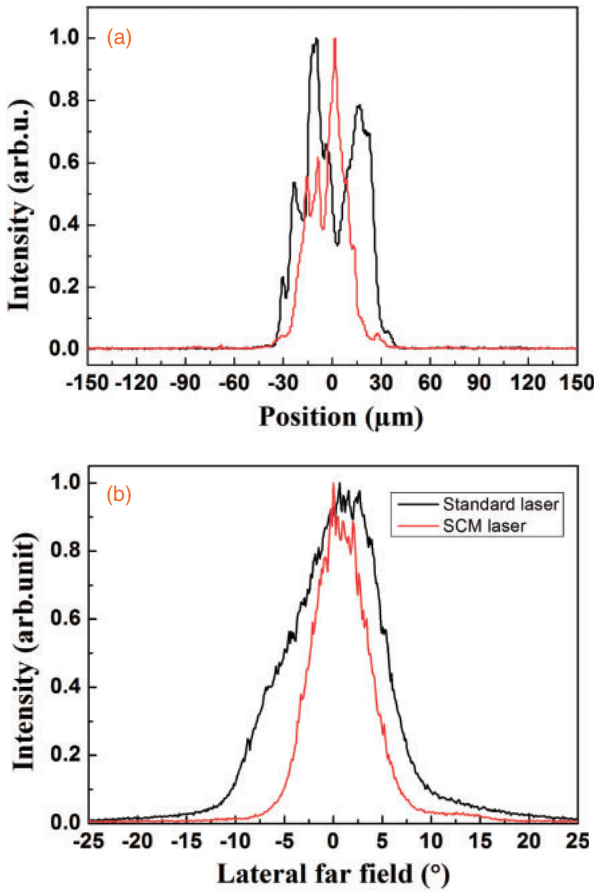

Fig. 6. Lateral near-field (a) and far-field profiles (b) for the standard and SCM lasers at 2.5 A, respectively.

For the definition of lateral divergences including 95% power content ($\theta_L^{95\%}$), the situation is also similar.

Although a stable lateral divergence has been realized, an ideal source would be with both high power and high beam quality. The beam quality properties are typically described in terms of the beam parameter product (BPP), which can be defined as

$$\mathrm{BPP} = \frac{w_{95\%} \cdot \theta_{95\%}}{4}, \tag{1}$$

where $w_{95\%}$ and $\theta_{95\%}$ are the full waist width and far-field angle containing 95% of the emitted power, respectively. Figure 6 shows the near-field and far-field profiles at 2.5 A. It is obvious that the lateral beam properties have been improved. The emission intensity at the stripe edge in SCM lasers decreases, which indicates that the LCA effect is suppressed. However, $w_{95\%}$ only improves by 3.2% with values of 63 μm for the standard device and 61 μm for the SCM device. The $\theta_L^{95\%}$ values are 19.2 and 12.6° for the standard and SCM devices at 2.5 A, respectively. Therefore, the obtained $\mathrm{BPP}_{\mathrm{lat}}$ values are 5.28 mm × mrad and 3.35 mm × mrad for these two types of laser, respectively, which corresponds to a 36.5% improvement in the lateral BPP achieved by the introduction of the SCM microstructure.

The CW lasing spectra of these two kinds of devices were measured using an ANDO AQ6370C optical spectrum analyzer. Figures 7(a) and 7(b) show the experimental spectral map at currents of 300 to 800 mA with a step width of 10 mA. The lasing spectrum at 1.5 A is shown in Fig. 7(c). The FWHM-defined linewidth of the lasing spectra of the standard device is about 3.1 nm. In contrast, it is only 1.7 nm for the SCM device, which indicates a 45% narrowing. In addition, the center wavelength for the SCM device is 968 nm and quite stable; however, it is shifted for the standard laser by about 1 nm. The narrow linewidth and stable wavelength can be attributed to the successful suppression of high-order longitudinal modes, which can be explained by the simple "box" model.[20] The wavelength separation from the fundamental mode is mathematically expressed as

$$\Delta\lambda(q,s,m) = -\frac{\lambda_0^2}{2n_g}\left[\frac{q}{L} + \frac{(s^2-1)\lambda_0}{4nW^2} + \frac{(m^2-1)\lambda_0}{4nD^2}\right]. \tag{2}$$

Here, λ_0 is the wavelength of the fundamental mode. m (= 1, 2, 3, ...), s (= 1, 2, 3, ...), and q (= 0, 1, 2, ...) are the transverse, lateral, and longitudinal mode numbers, respectively. n_g is the group index and n is the effective refractive index. L, W, and D are the cavity length and the width and thickness of the active region, respectively. For the devices fabricated in this work, the wavelength separation for adjacent longitudinal modes is about 0.11 nm from Eq. (2); in contrast, it is only 7.1 pm for the lateral modes. Hence, the narrowing of the lasing spectra is mainly attributed to the

© 2016 The Japan Society of Applied Physics

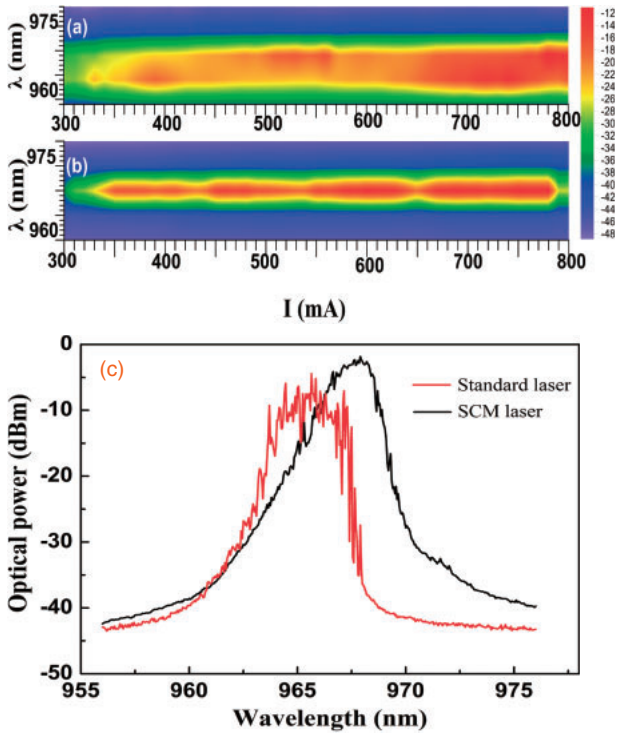

Fig. 7. Lasing spectra of BA lasers with (a) standard structure and (b) SCM structure operating under CW condition; (c) emission spectra of the two devices at 1.5 A.

suppression of high-order longitudinal modes, although the high-order lateral modes might also be suppressed. These explanations are consistent with the modulation intensity of carrier density in the lateral and longitudinal directions in SCM structures. As shown in Figs. 2 and 3, the carrier modulation in the longitudinal direction is much stronger than that in the lateral direction. Moreover, the strong periodical variation of optical gain along the longitudinal direction will filter some high-order longitudinal modes and result in the spectral narrowing.[21)]

In summary, a two-dimensional current modulation structure was proposed and its effectiveness for the control of far-field and lasing spectra in BA diode lasers was demonstrated. This structure can reduce the carrier density at the edge of the injection area, and injection-insensitive lateral divergence was realized without a very significant decrease in output power. About 45% narrowing in the linewidth of the lasing spectra was achieved owing to the SCM structure. With the combined low cost and compatibility with the fabrication techniques of diode lasers, the SCM structure is useful for the development of high-power BA diode lasers with low divergence and high beam quality.

Acknowledgments This work was supported by the National Natural Science Foundation of China (Nos. 61404138 and 61474119), International Science Technology Cooperation Program of China (No. 2013DFR00730), and Jilin Provincial Natural Science Foundation (Nos. 20140101203JC and 20150520105JH).

1) R. J. Lang, A. G. Larsson, and J. G. Cody, IEEE J. Quantum Electron. **27**, 312 (1991).
2) P. A. Kirkby, A. R. Goodwin, G. H. B. Thompson, and P. R. Selway, IEEE J. Quantum Electron. **13**, 705 (1977).
3) Z. Dai, R. Michalzik, P. Unger, and K. J. Ebeling, IEEE J. Quantum Electron. **33**, 2240 (1997).
4) A. I. Bawamia, B. Eppich, K. Paschke, H. Wenzel, F. Schnieder, G. Erbert, and G. Tränkle, Appl. Phys. B **97**, 95 (2009).
5) J. Piprek, Proc. SPIE **8619**, 861910 (2013).
6) J. Piprek and Z. M. Simon Li, Appl. Phys. Lett. **102**, 221110 (2013).
7) R. Craig, L. Casperson, J. Yang, G. Evans, and R. Davis, Electron. Lett. **21**, 62 (1985).
8) R. J. Lang, K. M. Dzurko, A. Hardy, S. Demars, A. Schoenfelder, and D. F. Welch, IEEE J. Quantum Electron. **34**, 2196 (1998).
9) S. Kallenbach, M. T. Kelemen, R. Aidam, R. Losch, G. Kaufel, M. Mikulla, and G. Weimann, Proc. 17th Annu IEEE Conf. Laser and Electro-Optics Society, 2004, p. 473.
10) H. Wenzel, K. Paschke, O. Brox, F. Bugge, J. Fricke, A. Ginolas, A. Knauer, P. Ressel, and G. Erbert, Electron. Lett. **43**, 160 (2007).
11) D. Heydari, Y. Bai, N. Bandyopadhyay, S. Slivken, and M. Razeghi, Appl. Phys. Lett. **106**, 091105 (2015).
12) H. C. Eckstein, M. Stumpf, U. D. Zeitner, C. Lauer, A. Bachmann, and M. Furitsch, Proc. IEEE Int. Semiconductor Laser Conf., 2014, p. 17.
13) D. Fendler, M. Spiegelberg, M. Moehrle, and W. Rehbein, Proc. IEEE Conf. Photonics Society Summer Top. Meet. Ser., 2012, p. 39.
14) P. Crump, P. Leisher, T. Matson, V. Anderson, D. Schulte, J. Bell, J. Farmer, M. Devito, R. Martinsen, Y. K. Kim, K. D. Choquette, G. Erbert, and G. Tränkle, Appl. Phys. Lett. **92**, 131113 (2008).
15) S. K. Sheem and B. A. Vojak, J. Appl. Phys. **63**, 248 (1988).
16) G. Sobczak, E. Dabrowska, M. Teodorczyk, K. Krzyzak, and A. Malag, IEEE J. Quantum Electron. **50**, 890 (2014).
17) M. Winterfeldt, P. Crump, S. Knigge, A. Maaßdorf, U. Zeimer, and G. Erbert, IEEE Photonics Technol. Lett. **27**, 1809 (2015).
18) LASTIP (Crosslight Software Inc., Burnaby, BC, 2010) [www.crosslight.com].
19) L. Borruel, S. Sujecki, P. Moreno, J. Wykes, P. Sewell, T. Benson, E. Larkins, and I. Esquivias, IEEE J. Quantum Electron. **40**, 1384 (2004).
20) H. S. Sommers, J. Appl. Phys. **44**, 1263 (1973).
21) J. Decker, P. Crump, J. Fricke, A. Maaßdorf, G. Erbert, and G. Tränkle, IEEE Photonics Technol. Lett. **26**, 829 (2014).

© 2016 The Japan Society of Applied Physics